

# Dark Matter implications of the Fermi-LAT measurement of anisotropies in the diffuse gamma-ray background: status report

Mattia Fornasa<sup>a,b</sup>, Jesus Zavala<sup>c</sup>, Miguel A. Sánchez-Conde<sup>d</sup>, Francisco Prada<sup>a</sup>, Mark Vogelsberger<sup>e</sup>

<sup>a</sup>*Instituto de Astrofísica de Andalucía - CSIC, Glorieta de la Astronomía, E-18008, Granada, Spain*

<sup>b</sup>*MultiDark fellow*

<sup>c</sup>*Department of Physics and Astronomy, University of Waterloo, 200 University Avenue West, Waterloo, Canada*

<sup>d</sup>*KIPAC - SLAC National Accelerator Laboratory, 2575 Sand Hill Road, Menlo Park, CA 94025, USA*

<sup>e</sup>*Harvard-Smithsonian Center for Astrophysics, 60 Garden St., Cambridge, MA 02138, USA*

---

## Abstract

For the first time, the Fermi-LAT measured the angular power spectrum (APS) of anisotropies in the diffuse gamma-ray background. The data is found to be broadly compatible with a model with contributions from the point sources in the 1-year catalog, the galactic diffuse background, and the extragalactic isotropic emission; however deviations are present at both large and small angular scales. In this study, we complement the model with a contribution from Dark Matter (DM) whose distribution is modeled exploiting the results of the most recent  $N$ -body simulations, considering the contribution of extragalactic halos and subhalos (from Millenium-II) and of galactic substructures (from Aquarius). With the use of the Fermi Science Tools, these simulations serve as templates to produce mock gamma-ray count maps for DM gamma-ray emission, both in the case of an annihilating and a decaying DM candidate. The APS will then be computed and compared with the Fermi-LAT results to derive constraints on the DM particle physics properties. The possible systematic due to an imperfect model of the galactic foreground is also studied and taken into account properly. The present paper reports on the status of the project.

*Keywords:* Dark Matter, anisotropies

---

## 1. Introduction

The Isotropic Gamma-Ray Background (IGRB) can be defined as the radiation that remains after the resolved sources (both point-like and extended) and the galactic foreground (produced from the interaction of the cosmic rays with the interstellar medium) are subtracted from the total gamma-ray emission. The most recent measurement of the IGRB energy spectrum was done by the Fermi-LAT telescope and presented in Refs. [1, 20]. Contrary to what was found by the EGRET telescope [3, 4], the IGRB appears to be perfectly compatible with a power-law with a slope of  $-2.41$ , at least up to 10 GeV.

The contribution of unresolved sources, both extragalactic (e.g., blazars [5, 6, 7, 8, 9, 10, 11], star-forming galaxies [6, 12] and radio galaxies [14, 13]) and galactic sources (like milli-second pulsars [15]) have been considered. The contribution of each class is estimated from population studies of the detected objects (see Ref. [11] for an example in the case of blazars) and it turns out that all the components considered up to now may not be able to account for the whole IGRB [16]. Thus there may be room for additional contributions like, e.g., that of Dark Matter (DM) [17, 18, 9, 19, 2]. Actually, the authors of Ref. [2] have already used the Fermi-LAT measurement of the IGRB intensity to constrain the properties of the DM particle, finding that, in their most optimistic scenario,

values larger than  $10^{-26} \text{cm}^3 \text{s}^{-1}$  for the annihilation cross section ( $\sigma_{\text{ann}} v$ ) can be excluded.

Complementary to the energy spectrum of the IGRB, we can also the recent analysis of the angular power spectrum (APS) of anisotropies in the diffuse gamma-ray background [21, 22, 23] to study the nature of the IGRB. The analysis was conducted by the Fermi-LAT collaboration and resulted in the detection of some angular power above multipoles of  $\ell > 155$ , with a significance larger than  $3\sigma$ , in the each of the energy bins between 1 GeV and 10 GeV. More detailed information on this measurement will be provided in Sec. 2. We simply note here that, even if such a detection seems to be compatible to the signal predicted for a population of unclustered, unresolved blazars, it can still be used to put some useful constraints on the nature of the DM particle. The goal of the present work is to derive those constraints using state-of-art numerical simulations.

The project is divided in two parts: in the first one we will make use of the most recent results from  $N$ -body simulations to derive all-sky maps of gamma-ray emission from DM annihilations and decay. We will consider the contributions of *i*) extragalactic halos and subhalos (based on the Millennium II  $N$ -body simulation [24]), *ii*) the emission from the smooth halo of the Milky Way (modeled as in Ref. [25] and *iii*) its subhalos (from the results of Aquarius [26, 27]). Moreover, we will also consider the emission

from halos and subhalos below the mass resolution of the two simulations mentioned above, down to the minimal halo mass  $M_{\min}$ . The all-sky maps will then be used to compute the APS of anisotropies in the gamma-ray emission from DM annihilation and decay. We plan to present the results of this first part in Ref. [28], where we will also study the dependence of the APS from the assumptions made while building the maps of DM-induced gamma-ray emission. Refer also to Secs. 3 and 4 for more information on this first part.

The second part of the project will deal with the comparison with Fermi-LAT APS data. The simulation maps produced in Ref. [28] will be used as templates for the DM contribution to the IGRB. We will use the most recent Fermi Instrument Response Functions (IRFs) to estimate how experimental issues may affect the APS. It will be particularly important to take correctly into account the experimental Point Spread Function (PSF) and the Fermi-LAT exposure. We will finally use the APS measurement to derive constraints on the nature of DM taking into account also the constraints from the new measurement of the IGRB energy spectrum (see also Sec. 5).

We will conclude this small introduction reminding that this note should be considered just as a status report, since none of the two parts of the project is complete up to now. We will present some preliminary results in Secs. 3 and 4, but we will mainly focus here on the methodology, emphasizing that the final results will be extensively presented in the near future [28].

## 2. Fermi-LAT measurement of the anisotropies in the diffuse gamma-ray background

For the analysis in Ref. [23] the first 22 months of Fermi-LAT data have been analyzed, dividing the energy range between 1 GeV and 50 GeV in 4 energy bins. The point sources in the first 1 year catalog [29] have been masked, as well as the emission within a band of 30 degrees above and below the galactic plane. This was done to cover the regions in the sky where the emission is dominated by resolved sources and by the galactic foreground, and to restrict the analysis only to where the IGRB is a significant component. We note here that the analysis performed in Ref. [20] to measure the IGRB intensity spectrum is different since templates of emission are implemented to subtract known components in the gamma-ray emission, instead than masking portions of the sky. Thus, strictly speaking, the data used in Ref. [23] and analyzed to derive the APS are not the same used for the IGRB energy spectrum in Ref. [20]. Moreover, even at high latitudes ( $|l| \geq 30^\circ$ ) the galactic emission is still important and non-negligible. We therefore expect that some level of contamination in the APS may be present from this kind of background. These contaminations are supposed to be located primarily at low angular multipoles  $\ell$  (large angular scales) and so only multipoles larger than 155 have

been considered in Ref. [23]. On the other hand, multipoles larger than 504 are also discarded since, at these small angular scales, the signal is strongly damped by the experimental PSF.

Two definitions of APS are used: *i*) the intensity APS as in Eqs. 1 and 2 below, for which the intensity gamma-ray maps are decomposed directly in spherical harmonics

$$a_{\ell,m} = \int I(\Psi) Y_{\ell,m}^*(\Psi) d\Omega, \quad (1)$$

$$C_\ell = \sum_{-|\ell|}^{|\ell|} |a_{\ell,m}|^2, \quad (2)$$

and *ii*) the fluctuation APS, that can be derived by the intensity one, dividing for the average intensity squared.

As a consequence, the fluctuation APS will not depend on the energy of the emission, if the distribution of the sources is energy-independent.

The Fermi-LAT reported detection of angular power in all the 4 energy bins considered, with a significance of larger than  $3\sigma$  in the energy bins from 1 GeV to 10 GeV. The data have been compared with the power spectrum of a *source model* made of *i*) the point-like sources in Ref. [29], *ii*) a model for the galactic foreground and *iii*) an isotropic component at the level of the IGRB in Ref. [20]. In the same regions outside the mask defined above, the general features in the APS of the model are similar to those in the data, but the model APS does not accurately reproduce the data APS in all energy bins on small or large angular scales. Furthermore, the model angular power at  $155 \geq \ell \geq 504$  is consistently below that measured in the data.

This seems to point to the possibility of having a population of unresolved sources contributing to the APS, in order to explain the data. The fact that the intensity APS is compatible with being independent of multipole, together with the way the intensity and fluctuation APS changes in the 4 energy bins suggests that one or more populations of unresolved, unclustered classes of sources may be responsible for the missing power.

If this hypothesis is true, then the data will provide us some useful constraints on the DM particle: the normalization and shape of the APS from DM annihilation has been studied extensively in the last years, focusing on the case of extragalactic halos and subhalos [18, 9, 30, 31, 32], on the case of a galactic component [34, 33, 10] or both [19, 35]. Comparing model predictions with the Fermi-LAT APS data allows us to put constraints on how important are DM-induced gamma-rays in the IGRB and, consequently, draw exclusion lines on the annihilation cross section, or other quantities more difficult to constrain like the minimal halo mass  $M_{\min}$ .

## 3. Extragalactic halos and subhalos

This section and the next one will be devoted to describe the methodology that will be used to compute the

maps of DM-induced radiation. To model the extragalactic emission, we use the catalogs of halos and subhalos of the Millennium-II  $N$ -body simulation: the simulation box is a cube with a size of  $100 \text{ Mpc}/h$  and it contains DM halos and subhalos down to a mass resolution of  $M_{\text{res}} = 6.89 \times 10^6 M_{\odot}/h$  [24]. Halo catalogs are available at multiple snapshots with different redshifts up to  $z = 127$ . We analyze them in a very similar way to what has been done in Ref. [32]: we will only consider objects with more than 100 particles and derive the properties of each halo (DM profile, luminosity and concentration) from the maximal circular velocity  $V_{\text{max}}$  and radius  $r_{\text{max}}$  (corrected from spurious effects related to numerical resolution, as done in Ref. [32]) and assuming a Navarro-Frenk-White (NFW) profile [36]. Since we want to probe a volume which is much larger than the Millennium-II simulation box, we implement the same technique described in Ref. [32] to construct sky-maps of the extragalactic signal, dividing the past light-cone in concentric shells (each of them at a particular redshift) and then filling them up with identical copies of the Millennium-II simulation boxes at that particular redshift (see Fig.9 in Ref. [32]). Each cube is randomly rotated and translated in order to avoid any boundary effect. In this way one can compute the luminosity from a particular direction in the sky  $\Psi$  simply by accounting for all the halos encountered in the direction of  $\Psi$ . This was done for all halos above Millennium-II mass resolution and you may see the results in Fig. 1 up to a  $z = 2.6$ .

We also want to consider the contribution of halos and subhalos below the mass resolution of Millennium-II. We treated main halos and subhalos separately and in two different ways. We will start by describing how we account for main halos with a mass smaller than  $M_{\text{res}}$ . Actually, the authors of Ref. [32] already considered this contribution: fitting the Millennium-II halos, they derived the cumulative luminosity function  $F(M) = \sum L/\bar{M}\Delta \log M$ , providing the total luminosity of main halos with a mass between  $M$  and  $M + dM$ . Then, they assumed that  $F(M)$  can be extrapolated below  $M_{\text{res}}$  in order to compute the gamma-ray flux predicted from main halo between  $M_{\text{min}}$  and  $M_{\text{res}}$ . This quantity was then used to boost up the luminosity of halos with a mass between  $1.4 \times 10^8 M_{\odot}/h$  and  $6.89 \times 10^8 M_{\odot}/h$ . This was done under the assumption that the distribution of main halos below  $M_{\text{res}}$  follows exactly that of those between  $1.4 \times 10^8 M_{\odot}/h$  and  $6.89 \times 10^8 M_{\odot}/h$ , such an approach is by the fact that the two-point correlation function (which is an indicator of clustering) is found to reach a constant value when approaching  $M_{\text{res}}$  (see Fig. 10 of Ref. [24]).

We want to test this assumption by implementing a different way of including the contribution of halos below  $M_{\text{res}}$ . We will then look for differences in the APS to check if the approach used to cover the range between  $M_{\text{min}}$  and  $M_{\text{res}}$  affects in any sense the shape of the APS. We therefore proceeded as follows:

- divide the range between  $M_{\text{min}}$  and  $M_{\text{res}}$  in mass decades ( $M_i, M_{i+1}$ ). For each mass decade, we considered all the halos in the Millennium-II simulation box with a mass between  $1.4 \times 10^8 M_{\odot}/h$  and  $6.89 \times 10^8 M_{\odot}/h$  and assign to each of them a new mass between  $M_i$  and  $M_{i+1}$ , assuming masses follow a probability distribution equal to the halo mass function  $dn/dM$ .
- we also assign a luminosity to each of these halos. From these two quantities, we can completely derive the halo profile. In this way, we end up by having a box of simulated objects with masses between  $M_i$  and  $M_{i+1}$  distributed as those between in the range  $1.4 \times 10^8 - 6.89 \times 10^8 M_{\odot}/h$ .
- however, in the mass decades we are considering, the halo mass function will predict more halos than we have actually have in the simulated box. So, we stack together different copies of the box obtained in the previous point until we reach the correct number of halos. The different copies are randomly rotated one with respect to the other.
- the box that comes out from the stacking is used to fill up the region up to a maximal distance of  $R_{\text{max}}$ , defined as the distance above which all halos in a given mass decade become point-like. Maps are produced from this distribution of objects till  $R_{\text{max}}$ .
- for the regime beyond  $R_{\text{max}}$ , we do not consider any stacking, we simply take the boxes coming from point 2 of this list and create the sky-map from those. Multiple copies of the map are then stacked together till the desired flux is reached. Since we are now in the regime where halos are point-like, the procedure is similar to what has been done below  $R_{\text{max}}$  but without having to consider the 3D distribution of halos.

This procedure, in a sense, moves in the opposite direction to what has been done in Ref. [32] since we start by assuming that halos below  $M_{\text{res}}$  have the same distribution of those above, but then we pass through a lot of independent rotations so that, at the end, the final maps are expected to be more isotropic than those in Ref. [32]. Once we compute the APS from the two approaches we will be able to see if differences show up in the shape of the APS.

In Fig. 2 (left panel) the black crosses indicate the IGRB energy spectrum taken from Ref. [20]. The red points show the amount of flux produced in halos and subhalos above  $M_{\text{res}}$  until  $z = 2.6$  (those depicted in Fig. 1) in the case of annihilating DM (filled points) and decaying DM (empty points). If we also consider the emission below  $M_{\text{res}}$  (implemented as described in the list above) the emission increases to be that one of the green points. For annihilating DM the increase is approximately of an order of magnitude, while for decaying DM it is completely negligible (red and green empty points practically overlap).



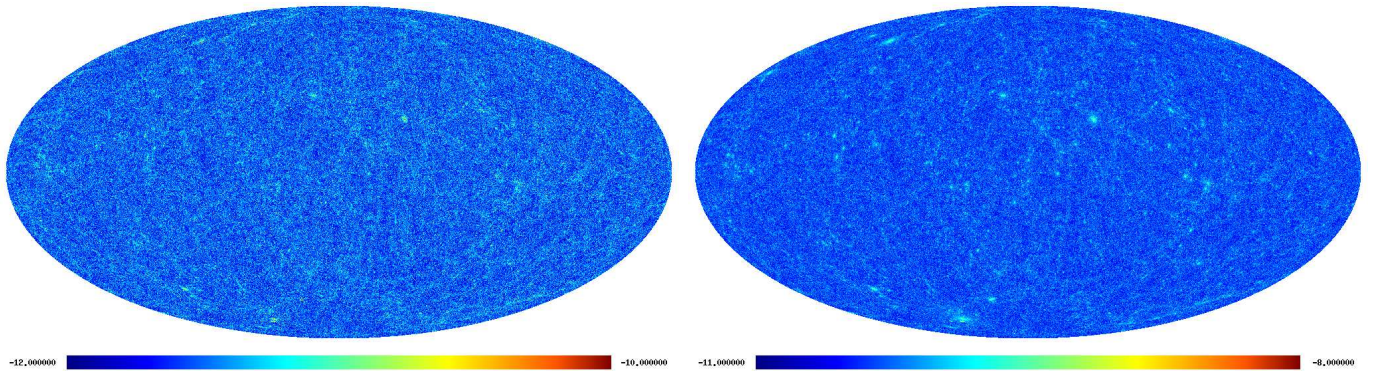


Figure 1: All-sky maps of gamma-ray emission from DM annihilation (left panel) or decay (right panel) in halos and subhalos above the mass resolution of Millennium-II, up to  $z = 2.6$ . Emission comes from hadronization of  $b$  quarks and is computed at 10 GeV. For the case of annihilating DM, the mass is 200 GeV and the annihilation cross section  $3 \times 10^{-26} \text{cm}^3 \text{s}^{-1}$ , while, for the decaying case, the mass is 2 TeV and the decay lifetime is  $\tau = 2 \times 10^{27} \text{s}$ .

The total flux is still a factor of 100 (50) for annihilation (decay) below the IGRB, at least at 10 GeV.

In order to complete the description of the extragalactic component, the only remaining ingredient is the emission from subhalos below  $M_{\text{res}}$ . Those will be described following the prescription derived in Ref. [37] and generalized in Ref. [38]. In the first reference the subhalos of the Via Lactea II  $N$ -body simulation are analyzed to compute the probability distribution  $P(\rho, r)$  of having a DM density between  $\rho$  and  $\rho + d\rho$  at a distance  $r$  from the center of the MW halo.  $P(\rho, r)$  has two distinct components: *i*) a parabolic regime due to the smooth halo and *ii*) a power-law that extends to larger densities due to substructures (see Fig. 1 of Ref. [37]). The authors, then used  $P(\rho, r)$  to compute the boost factor due to substructures, while Ref. [38] extended the prescription to halos larger and smaller than the MW halos, having in mind the case of galaxy clusters and dwarf Spheroidal galaxies respectively. We will use it to boost up the emission of the halos below  $M_{\text{res}}$ , accounting in this way for the emission of unresolved subhalos.

#### 4. The Milky Way halo and its subhalos

We continue now with the implementation of the gamma-ray emission related to our own galaxy: we use the distance of 700 kpc (approximately 3 times the virial radius of the Milky Way (MW) halo) as the limit between the extragalactic and the galactic regime.

The smooth halo of the MW is modeled with a NFW profile with parameters taken from Ref. [25], a model that is consistent with the available observation data on the MW. The total flux of the MW smooth halo is plotted in the left panel of Fig. 2. It represents the largest among the different DM components plotted there. However we should note that at the moment of computing the APS, we will mask the galactic plane, as it has been done by the Fermi-LAT collaboration in Ref. [23]. This will have

the effect of drastically decreasing the emission associated with the smooth halo.

To include the galactic subhalos we will use the Aquarius  $N$ -body simulation [27]. The same procedure described in the previous section will be used here for the Aquarius subhalos, without the need to considering replicas of the simulation box since we are interested only in the region within 700 kpc. The emission associated with galactic subhalos is indicated as yellow points in Fig. 2. We have not yet implemented the contribution of subhalos below the mass resolution of Aquarius  $M'_{\text{res}} = 1.712 \times 10^3 M_{\odot}$ . This will substantially increase the emission associated with galactic subhalos, which is only subdominant if we only consider objects above  $M'_{\text{res}}$ .

#### 5. Deriving constraints

The maps that will be obtained from the procedure sketched in the previous sections will then be used to compute the APS and to compare the results with the Fermi-LAT data. Some results can be seen in the central and right panels of Fig. 2 where the total fluctuation APS is plotted (black line). Also the contribution of the different components is present, multiplied by the square of the average flux of each component with respect to the total average emission, so that the sum of the colored lines gives the total (black line) also visually. Let us stress that these are very preliminary results: not all the components have been included (the contribution of unresolved extragalactic and galactic subhalos is missing) and we are not considering any mask.

We can, however, already see some interesting trends:

- the galactic component dominates the case of annihilating DM. This may change after we will include the contribution of galactic subhalos less massive than  $M'_{\text{res}}$ .
- the extragalactic component below  $M_{\text{res}}$  (both for annihilating and decaying DM) does not indicate any

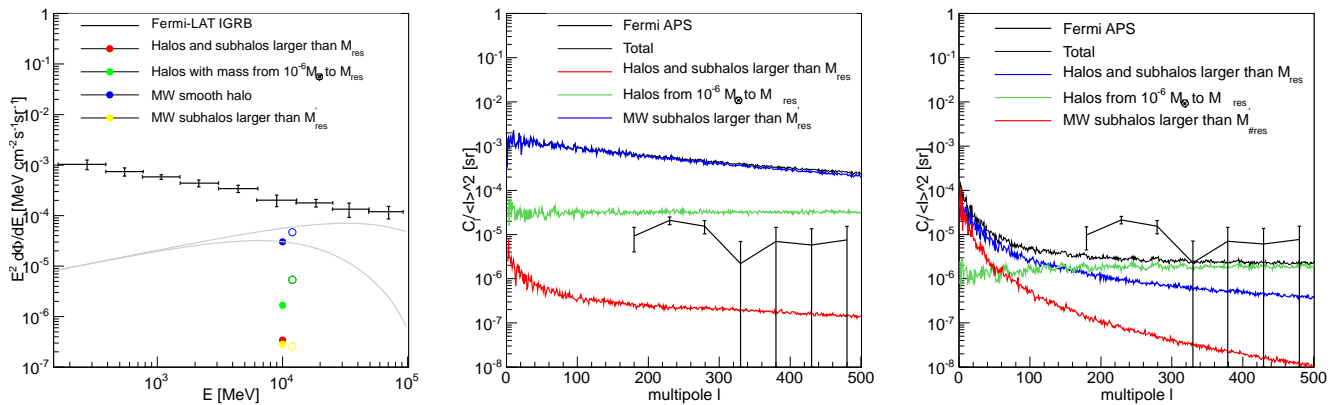


Figure 2: Left panel: Black crosses indicate the energy spectrum of the IGRB taken from Ref. [20]. Filled (empty) points refer to the case of annihilating (decaying) DM. Red points indicate the flux coming from DM halos and subhalos above  $M_{\text{res}}$ , while green points only consider the extrapolation down to  $M_{\text{min}}$  for main halos. Blue points show the emission from the smooth DM halo of the Milky Way, while the yellow ones accounts for the emission from all the subhalos in the Aquarius simulation. The grey lines refer to the annihilation and decay energy spectrum (from the hadronization of  $b$  quarks) normalized to blue points. Central and right panel: APS of anisotropies in the gamma-ray emission from DM annihilation (central panel) and decay (right panel). The total fluctuation APS is plotted in black, while the colored lines correspond to the different components, multiplied by the square of their average flux with respect to the total average flux. The red line indicates the contribution of extragalactic halos and subhalos above the mass resolution of Millennium II. The green line refers to main halos below  $M_{\text{res}}$  and down to  $M_{\text{min}}$ , while the blue one accounts for the subhalos in the Aquarius simulation.

intrinsic clustering, as expected.

- the contributions of Aquarius subhalos (blue lines) and of Millennium-II halos and subhalos (red lines) decrease with multipole, a consequence of the fact that the APS is sensitive to the inner structures of the halos.

In Fig. 2 we have also plotted the Fermi-LAT measurement of the fluctuation APS in the energy bin between 1 GeV and 2 GeV. Some other ingredients are still needed in order to be able to perform a proper comparison between the DM APS and the data. This will be done in the future, taking into account experimental features like the effect of the PSF, or a possible residual contamination from the Galactic foreground. We plan to include the IRF of the telescope using the Fermi Science Tools and treating the DM component in the same way as one of the three different components of the source model described in Sec. 2.

## 6. Conclusions

Here we briefly summarized a project which is still in progress. The goal is to compute realistic and complete all-sky maps of gamma-ray emission from DM annihilation and decay, taking into account the contribution of both extragalactic and galactic halos and subhalos. For the most massive objects we will refer directly to the results of two of the most recent  $N$ -body simulations (Millennium-II and Aquarius), but we will also account for smaller halos, down to their minimal mass  $M_{\text{min}}$ . Once obtained, these maps will be used to compute the APS of anisotropies. Our goal is to compare it with the recent measurement of the

APS by the Fermi-LAT collaboration in order to be able to put constraints on the nature of the DM particle. As the project is still on-going, we only presented here the methodology and some preliminary results. We refer interested readers to keep an eye on the arXiv webpage for the publication of the final results [28].

## Acknowledgements

The simulations used in this paper were carried out in the Cosmology Machine supercomputer at the Institute for Computational Cosmology, Durham. The Cosmology Machine is part of the DiRAC facility jointly funded by STFC, the Large Facilities Capital Fund of BIS and Durham University. We would also like to thank the Virgo Consortium for giving us access to the data of the Millennium-II and Aquarius simulations. Finally we thank the support of the Consolider-Ingénio 2010 Programme under grant Multi-Dark CSD2009-00064.

## References

- [1] <http://agenda.albanova.se/getFile.py/access?contribId=387&materialId=slides&confId=2600>
- [2] A. A. Abdo *et al.* [ Fermi-LAT Collaboration ], JCAP **1004** (2010) 014. [arXiv:1002.4415 [astro-ph.CO]].
- [3] P. Sreekumar *et al.* [ EGRET Collaboration ], Astrophys. J. **494**, 523-534 (1998). [astro-ph/9709257].
- [4] A. W. Strong, I. V. Moskalenko, O. Reimer, Astrophys. J. **613** (2004) 962-976. [arXiv:astro-ph/0406254 [astro-ph]].
- [5] F. W. Stecker, M. H. Salamon, Astrophys. J. **464** (1996) 600-605. [astro-ph/9601120].
- [6] V. Pavlidou, B. D. Fields, Astrophys. J. **575** (2002) L5-L8. [astro-ph/0207253].

- [7] T. Narumoto, T. Totani, *Astrophys. J.* **643** (2006) 81-91. [[astro-ph/0602178](#)].
- [8] S. 'i. Ando, E. Komatsu, T. Narumoto, T. Totani, *Mon. Not. Roy. Astron. Soc.* **376** (2007) 1635-1647. [[astro-ph/0610155](#)].
- [9] S. 'i. Ando, E. Komatsu, T. Narumoto, T. Totani, *Phys. Rev.* **D75** (2007) 063519. [[astro-ph/0612467](#)].
- [10] J. M. Siegal-Gaskins, V. Pavlidou, *Phys. Rev. Lett.* **102**, 241301 (2009). [[arXiv:0901.3776](#) [[astro-ph.HE](#)]].
- [11] T. F. -L. Collaboration, *Astrophys. J.* **720**, 435-453 (2010). [[arXiv:1003.0895](#) [[astro-ph.CO](#)]].
- [12] B. D. Fields, V. Pavlidou, T. Prodanovic, *Astrophys. J.* **722** (2010) L199. [[arXiv:1003.3647](#) [[astro-ph.CO](#)]].
- [13] Y. Inoue, *Astrophys. J.* **728**, 11 (2011). [[arXiv:1011.6511](#) [[astro-ph.HE](#)]].
- [14] Y. Inoue, *Astrophys. J.* **733**, 66 (2011). [[arXiv:1103.3946](#) [[astro-ph.HE](#)]].
- [15] C. -A. Faucher-Giguere, A. Loeb, *JCAP* **1001** (2010) 005. [[arXiv:0904.3102](#) [[astro-ph.HE](#)]].
- [16] [http://fermi.gsfc.nasa.gov/science/symposium/2011/program/session8/Ajello\\_FermiSymp\\_r.pdf](http://fermi.gsfc.nasa.gov/science/symposium/2011/program/session8/Ajello_FermiSymp_r.pdf)
- [17] P. Ullio, L. Bergstrom, J. Edsjo, C. G. Lacey, *Phys. Rev.* **D66**, 123502 (2002). [[astro-ph/0207125](#)].
- [18] S. 'i. Ando, E. Komatsu, *Phys. Rev.* **D73**, 023521 (2006). [[astro-ph/0512217](#)].
- [19] M. Fornasa, L. Pieri, G. Bertone, E. Branchini, *Phys. Rev.* **D80**, 023518 (2009). [[arXiv:0901.2921](#) [[astro-ph](#)]].
- [20] A. A. Abdo *et al.* [ The Fermi-LAT Collaboration ], *Phys. Rev. Lett.* **104** (2010) 101101. [[arXiv:1002.3603](#) [[astro-ph.HE](#)]].
- [21] G. G. Vargas, o. b. o. t. F. -L. collaboration, E. Komatsu, *Nuovo Cim.* **C34**, 03 (2011). [[arXiv:1012.0755](#) [[astro-ph.HE](#)]].
- [22] J. M. Siegal-Gaskins, f. t. F. -L. Collaboration, E. Komatsu, [[arXiv:1012.1206](#) [[astro-ph.HE](#)]].
- [23] [http://fermi.gsfc.nasa.gov/science/symposium/2011/program/session8/Siegal-Gaskins\\_Aniso\\_FermiSymp.pdf](http://fermi.gsfc.nasa.gov/science/symposium/2011/program/session8/Siegal-Gaskins_Aniso_FermiSymp.pdf)
- [24] M. Boylan-Kolchin, V. Springel, S. D. M. White, A. Jenkins, G. Lemson, *Mon. Not. Roy. Astron. Soc.* **398**, 1150 (2009). [[arXiv:0903.3041](#) [[astro-ph.CO](#)]].
- [25] F. Prada, A. Klypin, J. Flix Molina, M. Martinez, E. Simonneau, *Phys. Rev. Lett.* **93** (2004) 241301. [[astro-ph/0401512](#)].
- [26] J. F. Navarro, A. Ludlow, V. Springel, J. Wang, M. Vogelsberger, S. D. M. White, A. Jenkins, C. S. Frenk *et al.*, [[arXiv:0810.1522](#) [[astro-ph](#)]].
- [27] V. Springel, J. Wang, M. Vogelsberger, A. Ludlow, A. Jenkins, A. Helmi, J. F. Navarro, C. S. Frenk *et al.*, *Mon. Not. Roy. Astron. Soc.* **391** (2008) 1685-1711. [[arXiv:0809.0898](#) [[astro-ph](#)]].
- [28] M. Fornasa, J. Zavala, M. Vogelsberger, M. Boylan-Kolchin, C. S. Frenk, A. Jenkins, F. Prada, M. A. Sanchez-Conde, V. Springel, S. D. M. White, F. Zandanel *et al.*, in preparation.
- [29] A. A. Abdo *et al.*, *Astrophys. J. Suppl.* **188** (2010) 405.
- [30] A. Cuoco, S. Hannestad, T. Haugboelle, M. Kachelriess, P. D. Serpico, *Astrophys. J.* **676**, 807-815 (2008). [[arXiv:0709.2712](#) [[astro-ph](#)]].
- [31] A. Cuoco, J. Brandbyge, S. Hannestad, T. Haugboelle, G. Miele, *Phys. Rev.* **D77**, 123518 (2008). [[arXiv:0710.4136](#) [[astro-ph](#)]].
- [32] J. Zavala, V. Springel, M. Boylan-Kolchin, *Mon. Not. Roy. Astron. Soc.* **405**, 593 (2010). [[arXiv:0908.2428](#) [[astro-ph.CO](#)]].
- [33] J. M. Siegal-Gaskins, *JCAP* **0810**, 040 (2008). [[arXiv:0807.1328](#) [[astro-ph](#)]].
- [34] S. 'i. Ando, *Phys. Rev.* **D80** (2009) 023520. [[arXiv:0903.4685](#) [[astro-ph.CO](#)]].
- [35] A. Cuoco, A. Sellaerholm, J. Conrad, S. Hannestad, [[arXiv:1005.0843](#) [[astro-ph.HE](#)]].
- [36] J. F. Navarro, C. S. Frenk, S. D. M. White, *Astrophys. J.* **462** (1996) 563-575. [[astro-ph/9508025](#)].
- [37] M. Kamionkowski, S. M. Koushiappas, M. Kuhlen, *Phys. Rev.* **D81**, 043532 (2010). [[arXiv:1001.3144](#) [[astro-ph.GA](#)]].
- [38] M. A. Sanchez-Conde, M. Cannoni, F. Zandanel, M. E. Gomez, F. Prada, [[arXiv:1104.3530](#) [[astro-ph.HE](#)]].